Polymer Chemistry

PAPER

View Article Online
View Journal | View Issue



Cite this: *Polym. Chem.*, 2015, **6**, 7758

# The steric effect of α- and β-substituted anthraquinone units on high performance polymeric memory devices†

Hung-Ju Yen,‡§ Jung-Hsiang Chang,§ Jia-Hao Wu and Guey-Sheng Liou*

Received 13th August 2015,
Accepted 11th September 2015

DOI: 10.1039/c5py01285f

www.rsc.org/polymers

The new classes of anthraquinone-substituted triarylamine-based high-performance polymers have been successfully synthesized and fabricated for memory device application. The results show that the conformational change can effectively affect the retention time and memory behavior, providing a strategy for tailoring the memory characteristics through structural modulation.

## Introduction

The expedition in information technology at present has urged the development of novel materials for next-generation data-storage technologies.[1] Conventional Si-based technologies, which are common in the information storage area, are encountering the theoretical and physical extremes of minimization.[2] The emergent investigation for information storage in the form of high (ON) and low (OFF) current states instead of the amount of charges stored in silicon devices is to improve and enhance the superiority of higher data storage density, ease of miniaturization, tunable data retention time, faster speed, lower power consumption, and cost-effective processing for practical application.[1b] In order to develop outstanding memory devices with the above-mentioned parameters, there is an enormous effort in both worldwide industrial and academic areas currently. Extensive studies toward novel polymer materials and optimized device structures have been carried out to enhance memory performances, such as a large ON–OFF current ratio, low operation voltage, relatively long retention time, and high endurance.[3] Thus, polymeric memory devices have been developed as promising alternatives to the conventional semiconductor-based memory devices.

Among the polymer systems, aromatic polyimides (PIs) and polyamides (PAs) are considered as the most promising candidates for memory device applications owing to their excellent thermal stability, chemical resistance, and outstanding mechanical properties.[4] In addition, through the design and synthesis of organo-processable polymers, the electronic properties of a single polymer architecture with good chemical and physical properties can be successfully obtained, making the polymeric memory devices an intensively investigated research area. Triphenylamine (TPA) and its derivatives are well-known candidates as electron-donating materials when incorporated into the polymer backbone for polymeric memory devices due to their resulting stable radical cations, good hole-mobility, and high thermal stability.[4]

Recently, there have been several review articles summarizing the research progress of resistive memory devices.[3b,5] Among the reported polymers, most of the PIs or PAs have different molecular structures, which are difficult and insufficient to be investigated systemically for demonstrating the relationship between the polymer structures and their memory characteristics. How to predict the memory properties of the proposed structures prior to the measurement is still a difficult and crucial task. Thus, the design and synthesis of single donor–acceptor polymer architectures with similar but slightly different molecular features are supposed to be a great investigation to correlate the polymer structure and its memory characteristic.

In this work, we therefore synthesized two series of anthraquinone-triphenylamine (AQTPA)-based PIs and PAs from the diamine 1-(bis(4-aminophenyl)amino)anthracene-9,10-dione (α-diamine) and fabricated them for polymeric memory applications. AQ was chosen because the AQ-containing molecules are generally used in biochemistry for anti-cancer properties and conjugated polymers as an electron acceptor unit with a strong electron withdrawing characteristic.[6] AQs are the

*Functional Polymeric Materials Laboratory, Institute of Polymer Science and Engineering, National Taiwan University, 1 Roosevelt Road, 4th Sec., Taipei 10617, Taiwan. E-mail: gsliou@ntu.edu.tw; Fax: +886-2-33665237; Tel: +886-2-33665315*

† Electronic supplementary information (ESI) available: NMR spectra of dinitro, diamine, polyimide and polyamide. TGA, TMA, absorption, and calculated molecular orbitals of polymers. *In situ* absorption spectra of the memory devices. Table: viscosity, solubility, and thermal properties. See DOI: 10.1039/c5py01285f

‡ Present address: Physical Chemistry and Applied Spectroscopy (C-PCS), Chemistry Division, Los Alamos National Laboratory, Los Alamos, New Mexico 87545, USA.

§ H. J. Yen and J. H. Chang contributed equally to this work.

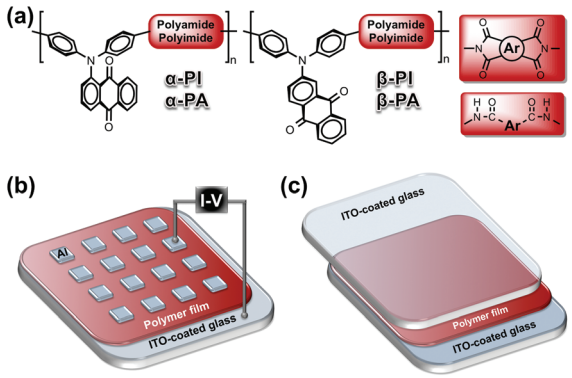


Fig. 1 (a) Chemical structures, (b) configuration of the memory device, and (c) configuration of the transparent device for "*in situ*" UV-vis absorption spectroscopy during switching-ON.

oxidized derivatives of aromatic compounds and are often readily made from reactive aromatic compounds with electron-donating substituents, such as phenols and catechol which increase the nucleophilicity of the ring and contributes to the large redox potential needed to break aromaticity. AQs are electrophilic Michael acceptors stabilized by conjugation due to the acceptor properties of the carbonyl groups. Therefore, the prepared AQTPA-based polymers are intrinsically donor–acceptor polymers. The memory devices fabricated with the configuration of indium-tin oxide (ITO)/polymer/Al were used to investigate the memory properties by *I–V* measurements and compared with the corresponding polymers prepared from **β-diamine**[7] as shown in Fig. 1. The isomeric AQTPA-based aromatic polymers with similar but elaborately varied molecular structures are beneficial to clarify the conformational and steric effects on their resulting memory characteristics.

## Results and discussion

### Monomer synthesis

The new AQTPA-functionalized monomer 1-(bis(4-aminophenyl)amino)anthracene-9,10-dione (**α-diamine**) was synthesized by hydrazine Pd/C-catalyzed reduction of the dinitro compound 1-(bis(4-nitrophenyl)amino)anthracene-9,10-dione (**α-dinitro**) resulting from the aromatic nucleophilic substitution reaction of α-aminoanthraquinone with 4-fluoronitrobenzene (Scheme 1). Elemental analysis, FT-IR and NMR spectroscopic techniques were used to identify structures of the intermediate **α-dinitro** and the target monomer **α-diamine**. The nitro groups of compound **α-dinitro** showed characteristic bands at around 1580 and 1308 $cm^{-1}$ due to $NO_2$ asymmetric and symmetric stretching. After reduction to the diamine monomer, the characteristic absorption bands of the nitro group disappeared and the primary amino groups revealed the typical absorption pair at 3464 and 3372 $cm^{-1}$ (N–H stretching). The $^{1}H$, $^{13}C$, two-dimensional COSY, HSQC NMR spectra of **α-dinitro** and **α-diamine** are illustrated in

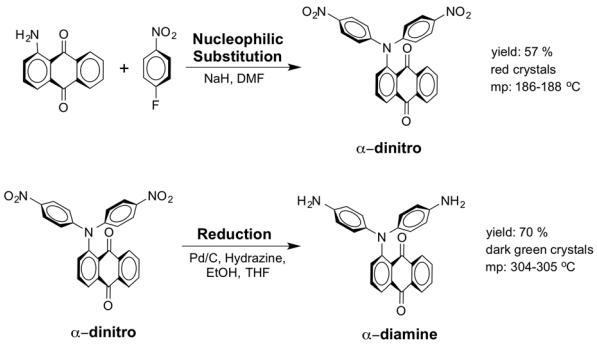


Scheme 1 Synthetic route to AQTPA-based diamine monomer **α-diamine**.

Fig. S1 to S4† and are in good agreement with the proposed molecular structures. Thus, the results of all the spectroscopic and elemental analyses suggest the successful preparation of the target diamine monomer.

### Polymer synthesis and basic characterization

The new **α-PI**s were prepared by one-step high-temperature solution polycondensation of **α-diamine** and three commercially available dianhydrides (Scheme 2). On the other hand, **α-PA**s were prepared by direct or low-temperature polycondensation as shown in Scheme 3. All the polymerization reactions proceeded homogeneously and gave highly viscous polymer solutions. The inherent viscosities, weight-average molecular weights, and polydispersity indices of the obtained polymers are summarized in Table S1.† All the polymers with high enough molecular weights afford transparent and free-standing films *via* solution casting (Schemes 2 and 3). The structures of the prepared polymers were identified by NMR spectroscopy, where the spectra are also in good agreement with the proposed molecular structures (Fig. S5 and S6†).

The solubility properties of polymers were qualitatively investigated at 5% w/v concentration and summarized in Table S2.† The high solubility of these polymers in polar aprotic organic solvents such as *N*-methyl-2-pyrrolidinone (NMP), *N*,*N*-dimethylacetamide (DMAc), and *N*,*N*-dimethylformamide (DMF) is attributable to the introduction of kinked and bulky α-(diphenylamino)anthracene-9,10-dione moieties

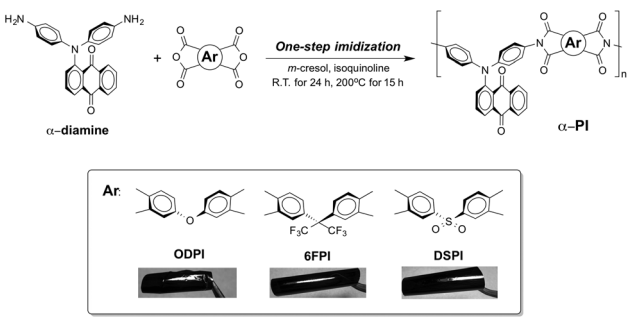


Scheme 2 Synthesis of AQTPA-based **α-PI**s.

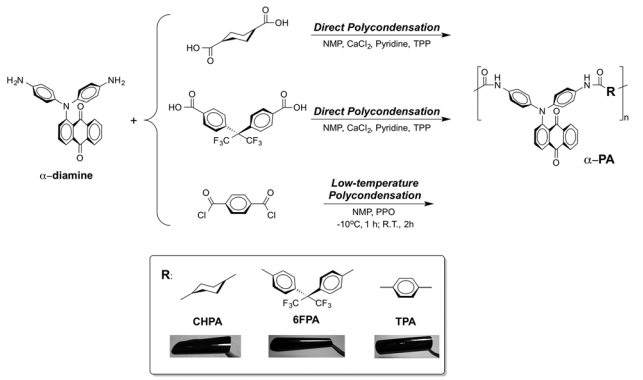


Scheme 3 Synthesis of AQTPA-based α-PAs.

into the polymer backbone. In addition, the excellent solubility of **α-6FPI** is due to the existence of the hexafluoroisopropylidene structure which limits the charge-transfer complex formation thus reducing the intermolecular interaction. On the other hand, the thermal properties of polymers were evaluated by thermogravimetric analysis (Fig. S7†) and using a thermal mechanical analyzer (Fig. S8†), and the data on thermal behavior are summarized in Table S3.† All the prepared polymers exhibit insignificant weight loss up to 400 °C under a nitrogen or air atmosphere, and the carbonized residue (char yield) under a nitrogen atmosphere of these polymers was more than 56% at 800 °C. The high thermal stability as well as glass transition temperature (up to 354 °C) can be ascribed to their high aromatic content.

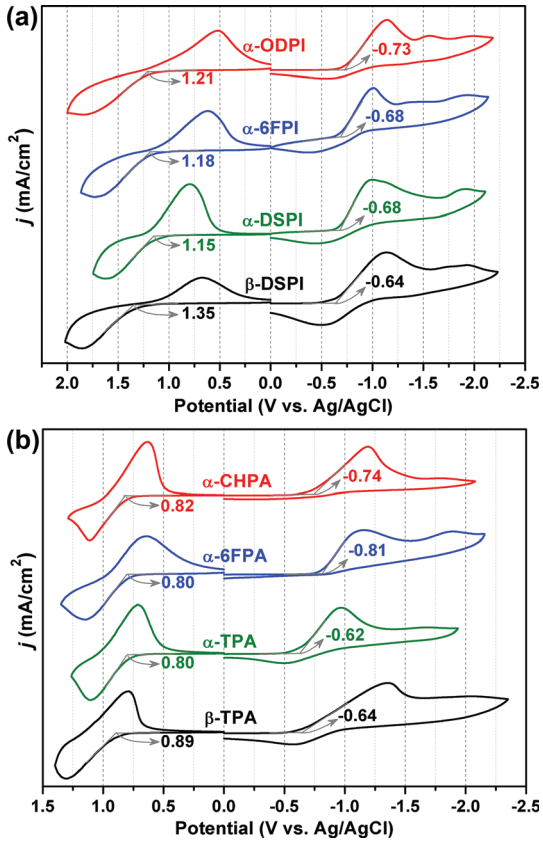


Fig. 2 Cyclic voltammetric diagrams of (a) PI and (b) PA films on an ITO-coated glass substrate.

### Optical and electrochemical properties

UV-vis absorption spectra of polymers are depicted in Fig. S9† and the onset wavelength of optical absorption was utilized to estimate the optical energy band gap. The electrochemical properties were investigated by cyclic voltammetry (CV) and using cast films on an ITO-coated glass slide as the working electrode. The typical CV for these polymers (Fig. 2) revealed one reversible oxidation redox couple. In addition, PIs and PAs exhibited three and two reduction peaks, respectively, and the difference is due to the additional reductive imide ring in PIs. The redox potentials of the polymers as well as their respective highest occupied molecular orbital (HOMO) and lowest unoccupied molecular orbital (LUMO) (*versus* vacuum) are calculated and summarized in Table 1.

### Memory device characteristics

The memory characteristics of these polymers were depicted by the current–voltage (*I–V*) curves of an ITO/polymer film/Al sandwich device as shown in Fig. 3 and 4. Within the sandwich device, polymer films were used as the active layer with Al and ITO as the top and bottom electrodes, respectively (Fig. 1b). The polymer film thickness was optimized around 50 nm and was used for all devices.

Fig. 3a–c summarize the *I–V* results of PIs **α-ODPI**, **α-6FPI**, and **α-DSPI**, respectively. Initially, the current of the as-fabricated device is low and no electrical switching capability could be observed when scanning positively (the first sweep). During the second negative sweep from 0 V to −6 V, the device stayed in the original OFF state with a current in the range $\sim 10^{-12}$ A followed by an abrupt increase to $10^{-4}$ A at the threshold voltage around −4.0 V, indicating the transition from the OFF state to the ON state. In a memory device, the OFF-to-ON transition can be defined as a "writing" process. The device retained in the ON state during the subsequent scan negatively (the third sweep) and then positively (the fourth sweep), meaning the reading process. The memory device could not be reset to the initial OFF state by applying a reverse electric field, implying the non-erasable memory behavior. In addition, the ON state could also remain once the memory devices have been switched to the ON state, even after turning off the power for an extended period of time (longer than one day).

These results depict that the α-based polyimides exhibit nonvolatile write-once-read-many-times (WORM) memory behaviors. On the other hand, the memory device based on **β-DSPI** shown in Fig. 3d exhibits a volatile static random-access memory (SRAM) behavior (12 min),[7] revealing a shorter retention time as opposed to the structural isomer **α-DSPI**.

Fig. 4 depicts the *I–V* curves of α-based PAs, **α-CHPA**, **α-6FPA**, **α-TPA**, and **β-TPA**, for comparison. Similar to the PIs,

 

Table 1 Redox potentials and energy levels of polymers

| | Thin films (nm) | | Oxidation[a] (V) | | Reduction[b] (V) | | | | | | Energy level | | |
|---|---|---|---|---|---|---|---|---|---|---|---|---|---|
| Code | $\lambda_{max}$ | $\lambda_{onset}$ | $E_{onset}$ | $E_{1/2}$ | $E_{onset}$ | $E^1_{1/2}$ | $E^2_p$ | $E^3_p$ | $E_g^{EC}$ (eV) | $E_g^{Opt}$ (eV) | $HOMO^{EC}$ [c] (eV) | $LUMO^{Opt}$ (eV) | $LUMO^{EC}$ (eV) |
| **α-ODPI** | 319 | 639 | 1.21 | 1.18 | −0.73 | −0.84 | −1.57 | −1.99 | 2.03 | 1.94 | 5.63 | 3.69 | 3.60 |
| **α-6FPI** | 301 | 617 | 1.18 | 1.18 | −0.68 | −0.69 | −1.36 | −1.94 | 2.03 | 2.01 | 5.62 | 3.61 | 3.59 |
| **α-DSPI** | 300 | 620 | 1.15 | 1.20 | −0.68 | −0.72 | −1.16 | −1.91 | 1.98 | 2.00 | 5.58 | 3.58 | 3.60 |
| **β-DSPI** | 307 | 565 | 1.35 | 1.18 | −0.64 | −0.82 | −1.73 | −1.93 | 1.98 | 2.19 | 5.65 | 3.46 | 3.67 |
| **α-CHPA** | 312 | 709 | 0.82 | 0.87 | −0.74 | −0.98 | −1.79 | — | 1.60 | 1.75 | 5.20 | 3.45 | 3.60 |
| **α-6FPA** | 336 | 700 | 0.80 | 0.90 | −0.81 | −1.01 | −1.89 | — | 1.75 | 1.77 | 5.22 | 3.45 | 3.47 |
| **α-TPA** | 339 | 708 | 0.80 | 0.91 | −0.62 | −0.75 | −1.69 | — | 1.49 | 1.75 | 5.19 | 3.44 | 3.70 |
| **β-TPA** | 322 | 606 | 0.89 | 0.89 | −0.64 | −0.97 | −2.04 | — | 1.65 | 2.05 | 5.32 | 3.27 | 3.67 |

$E_g^{EC}$ (Electrochemical band gap): difference between $HOMO^{EC}$ and $LUMO^{EC}$. $E_g^{Opt}$ (Optical band gap): calculated from polymer films ($E_g$ = 1240/$\lambda_{onset}$). $LUMO^{Opt}$ (LUMO energy levels calculated from the optical method): difference between $HOMO^{EC}$ and $E_g^{Opt}$. [a] *vs.* Ag/AgCl in $CH_3CN$. [b] *vs.* Ag/AgCl in DMF. [c] The HOMO and LUMO energy levels were calculated by cyclic voltammetry and were referenced to ferrocene (4.8 eV; $E_{onset}$ = 0.36 V in $CH_3CN$; $E_{1/2}$ = 0.52 V in DMF).

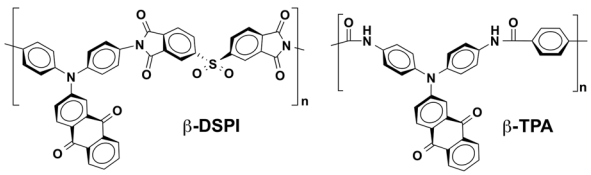


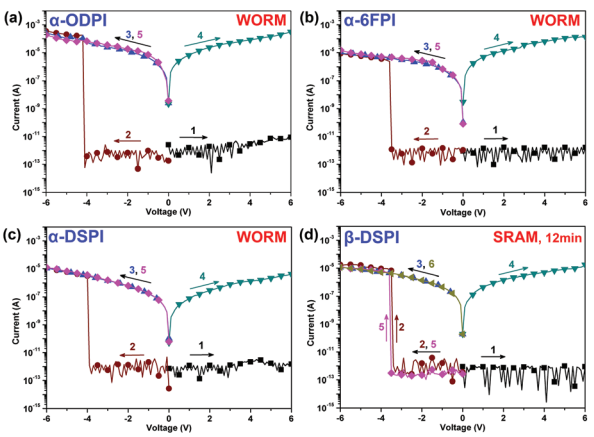


Fig. 3 Current–voltage (*I*–*V*) characteristics of the ITO/PI (50 ± 3 nm)/Al memory devices (a) **α-ODPI**, (b) **α-6FPI**, (c) **α-DSPI**, and (d) **β-DSPI**.

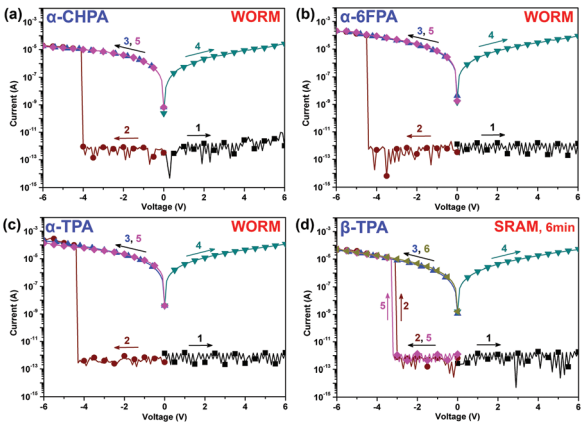


Fig. 4 Current–voltage (*I*–*V*) characteristics of the ITO/PA (50 ± 3 nm)/Al memory devices (a) **α-CHPA**, (b) **α-6FPA**, (c) **α-TPA**, and (d) **β-TPA**.

the α-based PAs also exhibited non-volatile WORM memory behaviors and **β-TPA** revealed a volatile SRAM behavior (6 min), respectively. For gaining more insight into the memory behaviors of the polymeric devices, the molecular orbital and electric density contours of the basic units were further estimated in detail by molecular simulation.

### Theoretical analysis and switching mechanism

The molecular simulation on the basic unit of AQ-based polymers was carried out by DFT/B3LYP/6-31G(d) with the Gaussian 09 program. The charge density isosurfaces of the basic unit, the most energetically favorable geometry, HOMO energy levels, and LUMO energy levels of all the polymers are depicted in Fig. 5, S10, and S11.† The results indicated that these two systems PIs and PAs revealed the charge transfer from the TPA donor (HOMO energy level) to the different α- and β- substituted electron acceptor AQ (LUMO energy level). When taking PIs as simulation models, the results showed that HOMO orbitals were localized at the triarylamine donor moieties, and LUMO orbitals were located at the electron-withdrawing AQ or diphthalimide units. As the applied potential reached the threshold voltage, electrons at the HOMO can accumulate energy to overcome the band gap and then transit to the LUMO 6 for **α-ODPI** and **α-6FPI** with the highest probability resulting in an excited state. Meanwhile, the electrons at the

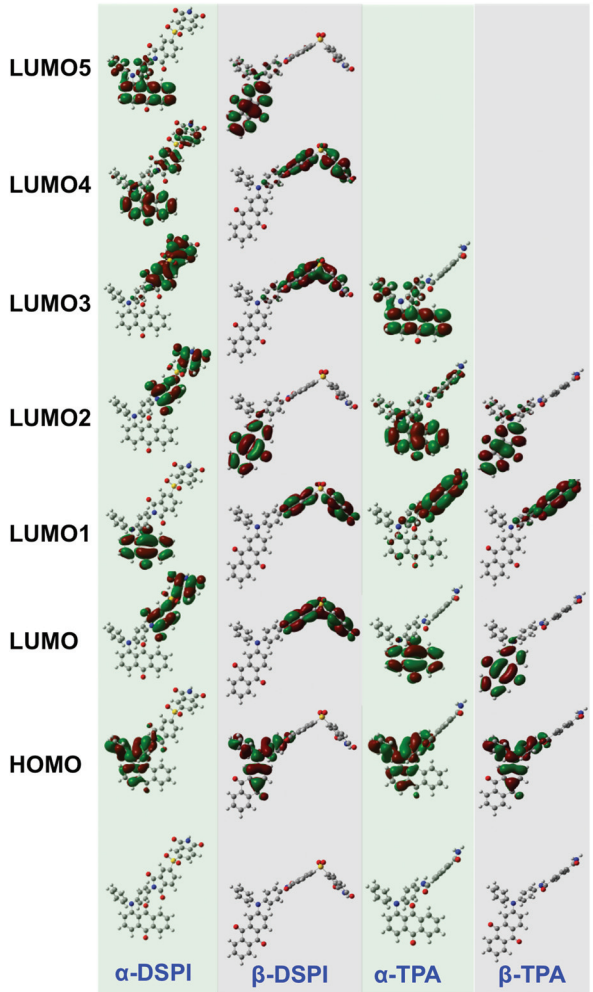


**Fig. 5** Calculated molecular orbitals and the corresponding energy levels of the basic units for **α-DSPI**, **β-DSPI**, **α-TPA**, and **β-TPA**.

HOMO orbital could also be excited to other LUMO orbitals with lower energy barriers. Therefore, charge transfer occurs through several routes to form the charge transfer complexes indirectly from the LUMO 6 through intermediate LUMOs then to the LUMO or directly from the HOMO to LUMO. For the intra- or intermolecular charge transfer complexes under the applied electric field, the generated holes at the HOMO can be delocalized within the donor moieties thus forming a conducting channel for the migration of charge carriers (holes). Thus, the current abruptly increases and the device can be switched to the ON state.

From the conformational point of view, the large torsion angle between the diphenylamine and AQ moieties could greatly stabilize the charge separation state, thus facilitating the energy barrier for the dissociation of the charge transfer complex and inhibiting the back charge recombination. Therefore, the results demonstrate that the conformational difference derived from steric hindrance can effectively affect the retention time and memory behavior from SRAM to WORM on changing the substituted anthraquinone from the β- to the α-position. It is worth mentioning that the **α-CHPA** obtained from alicyclic dicarboxylic acid also WORM behavior as other aromatic **α-PAs**, confirming that the charge transfer mechanism between the triarylamine donor and **α-AQ** acceptor moieties is the dominant factor for the interesting and peculiar memory behavior of the resulting **α-AQ** series polymers.

Furthermore, "*in situ*" UV-vis absorption spectroscopy during the switching-ON of **α-6FPI** and **α-6FPA** was utilized as direct evidence for field induced charge transfer memory behavior, which was carried out by using transparent devices as shown in Fig. 1c. Fig. S12a† depicts the UV-vis spectra of the device based on **α-6FPI** before and after switching to the ON state, and the absorption changes after turning off the power. By switching the device from the OFF to the ON state, the intensity of the absorption peak at around 350 nm increased, but the absorption peak could not return to the original absorption state even after turning off the device for 24 hours. While the absorption peak can be restored completely to the original OFF state by thermal treatment with 100 °C for 2–3 hours, the absorbance change was in good agreement with the non-volatile WORM memory properties. In addition, the absorbance changes of **α-6FPA** shown in Fig. S12b† revealed a similar result to PI **α-6FPI**, maintaining at the changed absorption for 4 days, and then it could be relaxed to the original absorption state by thermal annealing treatment. These "*in situ*" UV-vis absorption spectral measurements provide direct and solid evidence for the formation of the charge transfer complex, and make the field induced charge transfer an acceptable mechanism.

## Conclusion

The new classes of **α-AQ** substituted TPA-based high-performance polymers have been successfully synthesized and fabricated for memory device application. All the memory devices with the configuration of ITO/α-polymer film/Al exhibited WORM memory characteristics, while the corresponding memory devices based on β-polymers revealed SRAM properties. The results demonstrate that the conformational change from steric hindrance can effectively affect the retention time and memory behavior from SRAM to WORM by replacing the substituted anthraquinone from the β- to the α-position, providing a strategy to manipulate the memory characteristics through structural modulation.

## Acknowledgements

The authors gratefully acknowledge the Ministry of Science and Technology of Taiwan for financial support.

## Notes and references

1 (*a*) Q. D. Ling, D. J. Liaw, C. X. Zhu, D. S. H. Chan, E. T. Kang and K. G. Neoh, *Prog. Polym. Sci.*, 2008, **33**, 917;

 

(*b*) S. Moller, C. Perlov, W. Jackson, C. Taussig and S. R. Forrest, *Nature*, 2003, **426**, 166; (*c*) S.-T. Han, Y. Zhou and V. A. L. Roy, *Adv. Mater.*, 2013, **25**, 5425; (*d*) S. G. Hahm, T. J. Lee, D. M. Kim, W. Kwon, Y.-G. Ko, T. Michinobu and M. Ree, *J. Phys. Chem. C*, 2011, **115**, 21954; (*e*) H.-C. Wu, C.-L. Liu and W.-C. Chen, *Polym. Chem.*, 2013, **4**, 5261; (*f*) Y.-G. Ko, D. M. Kim, K. Kim, S. Jung, D. Wi, T. Michinobu and M. Ree, *ACS Appl. Mater. Interfaces*, 2014, **6**, 8415; (*g*) W. Elsawy, M. Son, J. Jang, M. J. Kim, Y. Ji, T.-W. Kim, H. C. Ko, A. Elbarbary, M.-H. Ham and J.-S. Lee, *ACS Macro Lett.*, 2015, **4**, 322; (*h*) Y.-H. Chou, H.-C. Chang, C.-L. Liu and W.-C. Chen, *Polym. Chem.*, 2015, **6**, 341.

2 S. Baek, D. Lee, J. Kim, S. H. Hong, O. Kim and M. Ree, *Adv. Funct. Mater.*, 2007, **17**, 2637.

3 (*a*) Q. D. Ling, F. C. Chang, Y. Song, C. X. Zhu, D. J. Liaw, D. S. Chan, E. T. Kang and K. G. Neoh, *J. Am. Chem. Soc.*, 2006, **128**, 8732; (*b*) T. Kurosawa, T. Higashihara and M. Ueda, *Polym. Chem.*, 2013, **4**, 16; (*c*) H.-J. Yen, C.-J. Chen and G.-S. Liou, *Adv. Funct. Mater.*, 2013, **23**, 5307; (*d*) J. Ouyang, C.-W. Chu, C. R. Szmanda, L. Ma and Y. Yang, *Nat. Mater.*, 2004, **3**, 918; (*e*) C. O. Baker, B. Shedd, R. J. Tseng, A. A. Martinez-Morales, C. S. Ozkan, M. Ozkan, Y. Yang and R. B. Kaner, *ACS Nano*, 2011, **5**, 3469; (*f*) Y. Yang, J. Ouyang, L. Ma, R. J. H. Tseng and C. W. Chu, *Adv. Funct. Mater.*, 2006, **16**, 1001.

4 (*a*) Y. Shirota, *J. Mater. Chem.*, 2005, **15**, 75; (*b*) Y.-H. Chou, N.-H. You, T. Kurosawa, W.-Y. Lee, T. Higashihara, M. Ueda and W.-C. Chen, *Macromolecules*, 2012, **45**, 6946.

5 (*a*) C.-L. Liu and W.-C. Chen, *Polym. Chem.*, 2011, **2**, 2169; (*b*) W.-P. Lin, S.-J. Liu, T. Gong, Q. Zhao and W. Huang, *Adv. Mater.*, 2014, **26**, 570.

6 (*a*) Q. Huang, G. Lu, H.-M. Shen, M. C. M. Chung and C. N. Ong, *Med. Res. Rev.*, 2007, **27**, 609; (*b*) J. Gheeya, P. Johansson, Q.-R. Chen, T. Dexheimer, B. Metaferia, Y. K. Song, J. S. Wei, J. He, Y. Pommier and J. Khan, *Cancer Lett.*, 2010, **293**, 124.

7 Y. C. Hu, C. J. Chen, H. J. Yen, K. Y. Lin, J. M. Yeh, W. C. Chen and G. S. Liou, *J. Mater. Chem.*, 2012, **22**, 20394.